DØ Note 5937-CONF

Search for pair production of the supersymmetric partner of the top quark in the $\tilde{t}\bar{\tilde{t}} \to b\bar{b}e^{\pm}\mu^{\mp}\tilde{\nu}\bar{\tilde{\nu}}$ decay channel at DØ

The DØ Collaboration
URL http://www-d0.fnal.gov
(Dated: June 13, 2009)

We report the result of a search for the pair production of the light top squark decaying to two bottom quarks, an electron, a muon, and two sneutrinos in 3.1 $\pm$ 0.2 fb^{-1} of data from the DØ detector at the Tevatron, Fermilab's $\sqrt{s}$ = 1.96 TeV $p\bar{p}$ collider. No significant excess of events above the standard model prediction was detected and new exclusion limits at the 95% confidence level have been set for a portion of the stop mass-sneutrino mass plane.

Preliminary Results for Summer 2009 Conferences

I. INTRODUCTION

In the Minimal Supersymmetric Standard Model (MSSM) [1], the mixing between the chiral states of the scalar partner particles of the standard model fermions is greatest for the top quark due to its large mass. Thus, it is possible that the light stop is the lightest squark and has the largest production cross section at the Tevatron. If R-parity is conserved, then the top squarks would be produced in pairs with the dominant diagrams being quark/anti-quark annihilation and gluon/gluon fusion, see Figures 1 and 2 respectively. If the two body decays $\tilde{t} \to b\tilde{\chi}^+$ and $\tilde{t} \to t\tilde{\chi}^0$ are kinematically forbidden, then the likely decay modes are the two body $\tilde{t} \to c\tilde{\chi}^0$, the three body $\tilde{t} \to b\tilde{\nu}^0\bar{l}^+$, and the four body $\tilde{t} \to b\tilde{\chi}^0 f\bar{f}$. We search for the three body decays of top squark pairs in the $b\bar{b}\ e^{\pm}\mu^{\mp}\tilde{\nu}\nu$ final state with the following assumptions: top squarks decay via the three body decay mode with a 100% branching fraction; R parity is conserved; and the sneutrino is the lightest supersymmetric particle or decays invisibly.

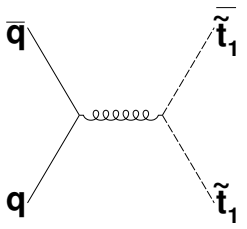

FIG. 1: Quark/anti-quark annihilation diagram for top squark pair production.

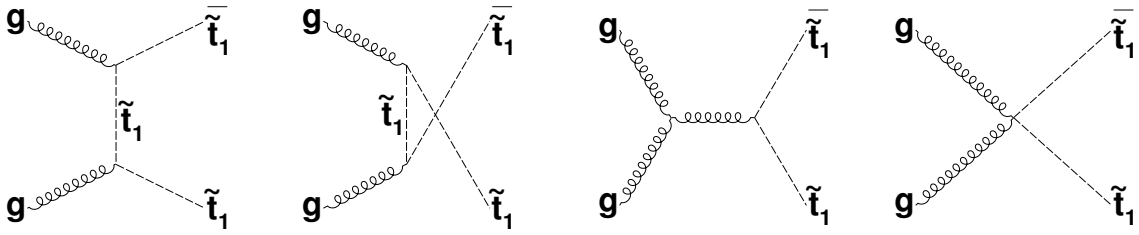

FIG. 2: Gluon/gluon fusion diagrams for top squark pair production.

II. DØ DETECTOR

The DØ detector has been described in detail elsewhere [2]. The main components of the detector include a central-tracking system located inside a 2T superconducting solenoid. The inner-most tracking element is the silicon microstip detector, followed by a scintillating fiber tracker. These two detectors together measure the momenta of charged particles. Outside the solenoid is the uranium-liquid argon calorimeter which is divided into a central calorimeter and two end-cap calorimeters. The final layer of the detector is the muon system, which consists of proportional drift tubes and scintillator trigger counters, followed by a 1.8T toroid, and two additional layers of drift tubes and scintillators.

III. DATA AND MONTE CARLO SAMPLES

This analysis studies 3.1 ± 0.2 fb^{-1} of the data collected by the DØ collaboration from June 2006 through December 2008. Events for the stop search (the "search data") were required to have an electron and a muon of opposite charge. The electron and muon were required to have p_T greater than 15 GeV and 8 GeV respectively. The $e\mu$ final state has relatively small standard model backgrounds, making this an excellent channel in which to search for new physics. The trigger efficiency is high for this combination of lepton p_T, and therefore no explicit trigger requirement is applied to the data events. Events from runs for which any of the detector subsystems had problems were removed to ensure data quality.

Monte Carlo events were produced to represent evenly spaced points on the stop mass-sneutrino mass plane. For each point, the MSSM particle mass and decay parameters were calculated with Suspect version 2.3 [3]. Madgraph/Madevent version 4.4.13 [4] was used to generate the four vectors for the signal events with Pythia version 6.409 [5]. to provide the showering and hadronization. The next-to-leading order (NLO) cross section for light top squark pair production was calculated by Prospino2.0 [6] with the CTEQ6.1M parton distribution function. The calculations were performed with the factorization and renormalization scales set to one, one half, and two times the stop mass in order to determine the nominal value and the negative and positive uncertainties. These theoretical uncertainties are combined quadratically with the PDF uncertainties [7][8] to give the positive and negative uncertainties for the signal cross section.

All the backgrounds in this analysis except for Quantum Chromodynamics multijet processes (QCD) are modeled using Monte Carlo events generated with Alpgen+Pythia[9] or Pythia. In order to simulate detector noise and multiple interaction effects, each Monte Carlo event is overlayed with a minimum bias data event from a random $p\bar{p}$ crossing. For a listing of the backgrounds and cross sections used for normalization, see Table I.

Background	Generator	σ (pb)
Z$\rightarrow l^+l^-$	Alpgen+Pythia	774
$t\bar{t}$	Alpgen+Pythia	$7.48^{+0.56}_{-0.73}$
W+jets$\rightarrow l\nu$+ jets	Alpgen+Pythia	8208
ZZ	Pythia	1.42±0.078
WZ	Pythia	3.68±0.25
WW	Pythia	12.0±0.67

TABLE I: The cross sections used to normalize the background Monte Carlo samples for this analysis. All cross sections are next-to-leading order except for $t\bar{t}$ which is scaled to the next to next-to-leading order cross section given in [10].

A. Object identification and QCD Backgound Sample

For all events the absolute value of the z component of the primary vertex was required to be less than 60 centimeters.

1. Jet Definition

For this analysis jets are reconstructed using the D0 RunII cone algorithm [11] with cone radius $\Delta\mathcal{R} = \sqrt{\Delta\phi^2 + \Delta\eta^2} < 0.5$. In this expression, ϕ is the azimuthal angle, η is the pseudorapidity ($\eta = -ln(tan(\theta/2))$), and θ is the polar angle with respect to the beam direction. Jet energies are corrected to the particle level. For a jet to be retained in an event it was required to have transverse energy $E_T > 15$ GeV and $|\eta| < 2.5$. Any jets for which $\Delta\mathcal{R}(jet, electron) < 0.5$ were removed. No explicit cut based on the the number of jets was applied. The missing transverse energy $\not\!\!E_T$ is computed from the calorimeter cells and is corrected for the jet energy corrections and the p_T of the reconstructed muon.

2. Electron Selection

Electrons were required to have transverse momentum greater than 15 GeV/c. The distance between the extrapolated z position of the electron track along the beam axis and the event primary vertex was required to be less than one centimeter. Electrons were required to have $|\eta| < 1.1$ as well as meet the following criteria:

- An isolation variable defined as $[E_{tot}(0.4) - E_{EM}(0.2))]/E_{EM}(0.2)$ was required to be less than 0.15. In this expression $E_{tot}(0.4)$ is the total calorimeter energy in a cone $\mathcal{R} < 0.4$ and $E_{EM}(0.2)$ is the calorimeter electromagnetic energy in a cone $\mathcal{R} < 0.2$ about the electron direction.
- 90% of the energy must be deposited in the electromagnetic portion of the calorimeter.
- The shower shape must be consistent with that of an electromagnetic shower.

- Electrons must be matched to a central track within a window $\Delta\eta \times \Delta\phi = 0.05 \times 0.05$ around the electromagnetic cluster.
- E/p < 2.5 where E is the calorimeter energy and p is the momentum in the tracking system.
- The eight variable likelihood function, which discriminates between electromagnetic and hadronic showers, must be greater than 0.85.

The central track is requuired to have $p_T > 5$ Gev/c. Events were required to have exactly one electron meeting these requirementsm, and the electron was required to have the opposite charge of the muon

3. Muon Selection

Muons are reconstructed in the region $\mid \eta \mid < 2$. The muon identification is broken down into three parts: muon system quality, tracking system quality, and calorimeter isolation. Selected muons were required to have both wire and scintillator hits in the muon system. The muon tracks were required to meet the following criteria:

- The χ^2 of the matched central track must be less than 4.0.
- If there were silicon microstrip tracker (SMT) hits, then the distance of closest approach (DCA) between the muon track and the primary vertex must be less than 0.02 cm.
- If there were no SMT hits, then DCA must be less than 0.2 cm.

Muons were required to meet the following isolation requirements:

- The energy in the calorimeter cone $0.1 < \Delta\mathcal{R} < 0.5$ around the muon track divided by the muon p_T must be less than 0.15.
- The sum of the transverse energy of the all the tracks in the cone $\Delta\mathcal{R} < 0.5$ around the muon track but excluding the muon track, divided by the p_T of the muon track must be less than 0.15.

In addition, muons were required to have $p_T > 8.0$ GeV/c. Events were required to have exactly one muon meeting these requirements. Further, events were rejected if $\Delta\mathcal{R}(jet_1, muon) < 0.5$ or $\Delta\mathcal{R}(e, \mu) < 0.5$ where jet_1 is the jet with the largest transverse energy in the event. Also, the distance between the extrapolated z position of the muon track along the beam axis and the event primary vertex was required to be less than one centimeter.

4. QCD Background

The QCD background sample is a selection of data events which is orthogonal to the search data. These events are required to have same sign charged leptons, and both the electron and muon are also required to fail some of the selection criteria described above. This sample is then scaled by the ratio of the number of QCD-like events in the search data divided by the number of events in the QCD background sample.

B. Event reweightings and object corrections

Correction factors derived from $Z \rightarrow ll$ $(l = e, \mu)$ data and Monte Carlo samples were applied to make resolutions consistent between data and Monte Carlo. Luminosity reweighting was applied to make the luminosity profile of the Monte Carlo minimum bias overlay events match the data sample. Beam spot reweighting was applied to make the primary vertex distribution of the Monte Carlo more similar to that of the data. Since the efficiency of electron and muon identification is higher for Monte Carlo than for data, corrections were applied for both. Smearing was applied to the energy of the jets and the momentum of the charged leptons to make the values more consistent with the data.

IV. EVENT SELECTION

The size of the mass difference between the light top squark and the sneutrino determines the kinematics of the final state. A larger difference will lead, on average, to more missing energy, larger amounts of jet energy, and higher p_T charged leptons. For optimization of this analysis, two benchmark points were chosen, (light stop mass in GeV/c^2, sneutrino mass in GeV/c^2) = (150,50) and (110,80) which will be referred to as the "hard" and "soft" benchmarks respectively.

Since there are many signal points and their characteristics differ greatly, the strategy for the selection cuts is to remove or isolate the backgrounds. The largest backgrounds are $Z \to \tau\bar{\tau}$, QCD, WW, and top quark pairs. Two cuts were applied to remove $Z \to \tau\bar{\tau}$ and QCD. The remaining events were distributed into a two dimensional histogram. The bin edges were selected to concentrate the WW and top quark pair events into a few bins so that the remaining bins could have a significant signal to background ratio.

A. Cut 1: Angular differences

The first cut was applied to remove $Z \to \tau\bar{\tau}$, the most significant background at the preselection level, as well as QCD background. The taus from $Z \to \tau\bar{\tau}$ usually have a significant boost from the initial Z boson decay. When the boosted taus decay into an electron and muon plus neutrinos, the electron and the muon are usually back-to-back. The measured $\not\!\!E_T$ is also usually back-to-back with one of the leptons. This effect can be seen in Figure 3. To reduce the $Z \to \tau\bar{\tau}$ contribution, events were required to meet the following criteria:

$$\Delta\phi(e, \not\!\!E_T) + \Delta\phi(\mu, \not\!\!E_T) > 2.9 \text{ radians and } \Delta\phi(e, \not\!\!E_T) > 0.4 \text{ radians and } \Delta\phi(\mu, \not\!\!E_T) > 0.4 \text{ radians.} \quad (1)$$

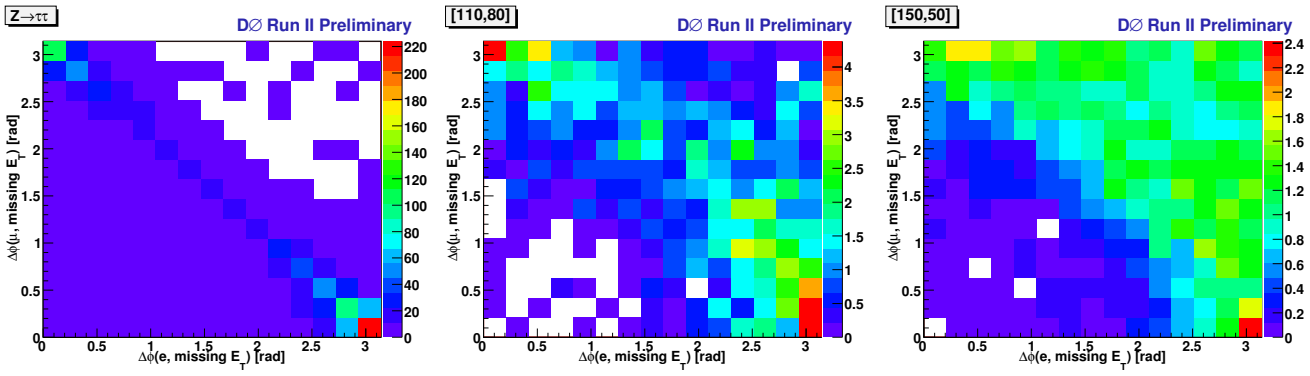

FIG. 3: The plots show $\Delta\phi(e, \not\!\!E_T)$ (vertical axis) and $\Delta\phi(\mu, \not\!\!E_T)$ (horizontal axis) for the $Z \to \tau\tau$ sample (left), the soft signal benchmark(middle), and the hard signal benchmark(right). For the $Z \to \tau\tau$ the $\not\!\!E_T$ is usually back to back with one of the leptons.

B. Cut 2: Missing Transverse Energy

After cut 1 the QCD and $Z \to \tau\tau$ backgrounds are dominant in the low $\not\!\!E_T$ region, see Figure 4. To reduce these backgrounds, we required $\not\!\!E_T > 18\ GeV$.

C. Kinematic Discrimination: H_T and S_T

The signal Monte Carlo events, the background Monte Carlo and QCD events, and the data events were sorted into 12 bins in the H_T (the scalar sum of the p_T of the jets) and S_T (the scalar sum of the $\not\!\!E_T$, the electron p_T, and the muon p_T) plane. The bins were chosen to try to isolate the WW and $t\bar{t}$ background into a few bins so that the signal to background ratio in the other bins would be maximized. The H_T bin edges were set to {0,15,70,170,1960} GeV. The bin edge at 15 GeV separates events which have a jet from those which do not. Most WW events do not

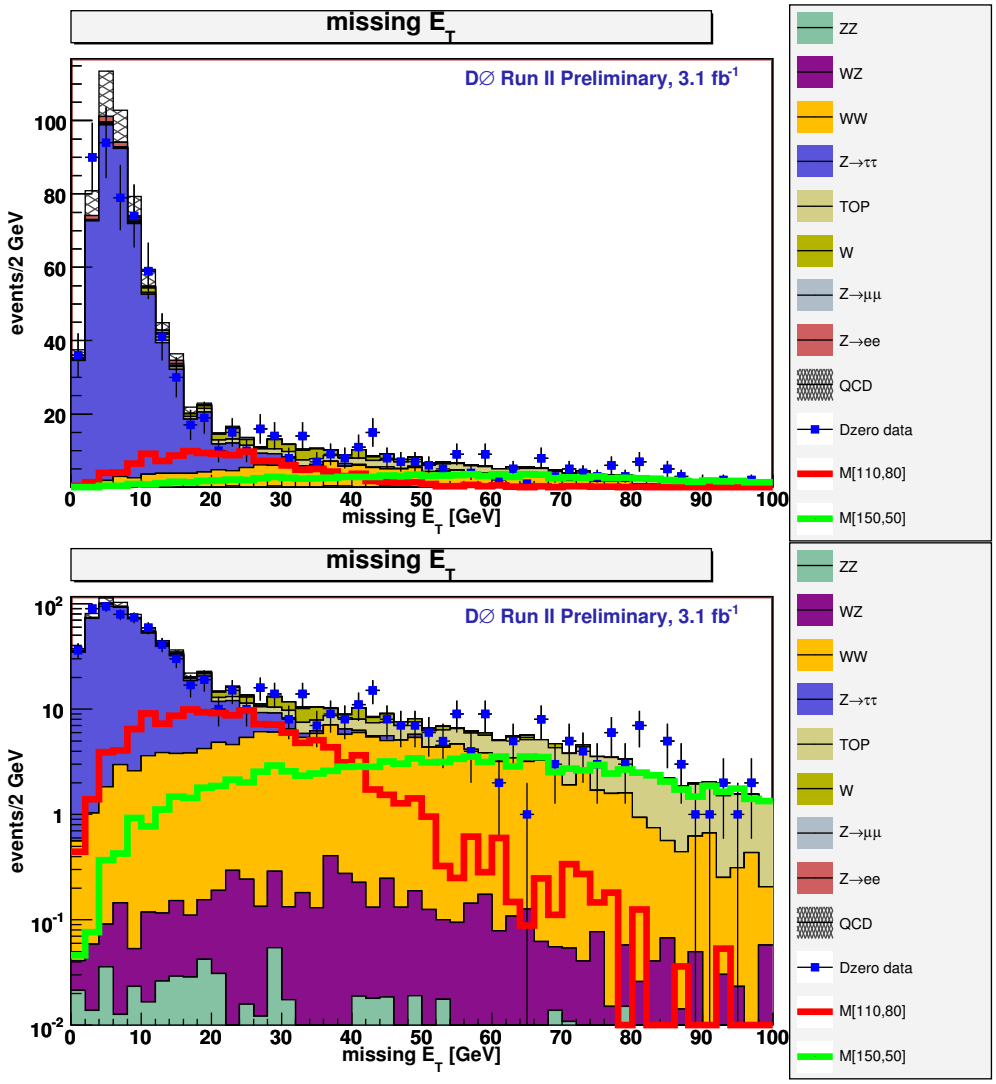

FIG. 4: Plots show data (points), Monte Carlo + QCD (filled areas), and the soft [$m_{\tilde{t}_1} = 110$ GeV/c^2, $m_{\tilde{\nu}} = 80$ GeV/c^2] and hard [$m_{\tilde{t}_1} = 150$ GeV/c^2, $m_{\tilde{\nu}} = 50$ GeV/c^2] signal benchmarks (lines) after the first cut has been applied in normal(top) and log scale(bottom). The second cut requiring $\not\!\!E_T > 18$ GeV will remove the region dominated by the QCD and $Z \to \tau\tau$ backgrounds.

have a jet and therefore have $H_T < 15.0$ GeV. Many signal events will fall in the range [15,70] GeV which separates them from the $t\bar{t}$ events which fall primarily in the range [70,170] GeV. The bin range [170,1960] GeV does not have many events but may be of value for signals with a small cross section but a large difference between the stop mass and the sneutrino mass.

The S_T bins were set to {0, 80, 220, 1960} GeV in order to isolate WW which is the primary background for the softer signal points after the first two analysis cuts. Most WW events have S_T between 80 and 220 GeV. Soft signal events will have S_T between 0 and 80 GeV, while the hardest ones will have $S_T > 220$ GeV.

This method of isolating the background without cutting it makes it possible to use the same set of cuts for many different signals. The distributions of H_T and S_T after the selection cuts are shown in Figure 5.

V. SELECTION SUMMARY

The results of the cuts and the efficiencies are shown in Table II. The first two selection cuts were chosen to favor acceptance over purity because further signal isolation is provided by the (H_T,S_T) bins. At the preselection level,

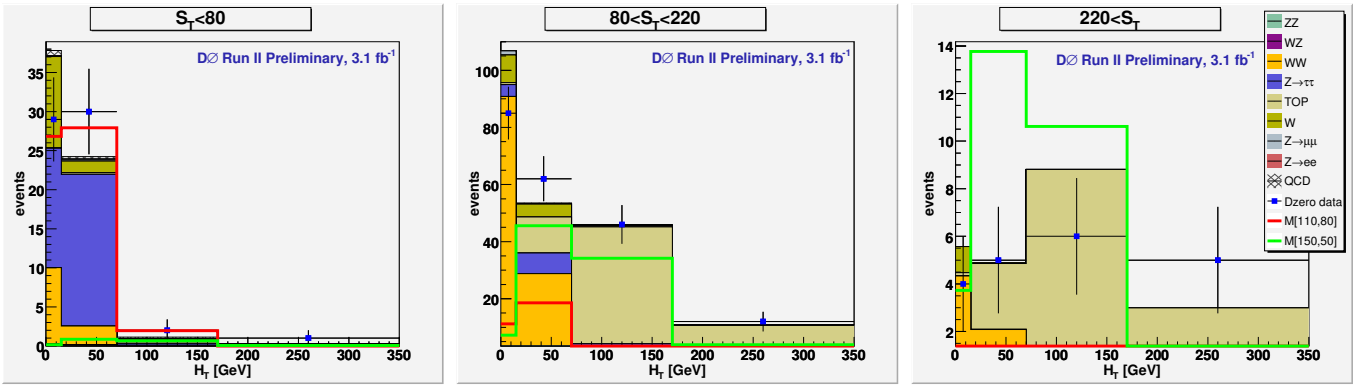

FIG. 5: The three figures show the H_T bins for $S_T < 80$ GeV (left), 80 GeV $< S_T <$ 220 GeV (middle) and $S_T > 220$ GeV (right). Data is represented as points; the Monte Carlo backgrounds as filled areas; the QCD as shaded area; and the soft $[m_{\tilde{t}_1} = 110\ \mathrm{GeV/c^2}, m_{\tilde{\nu}} = 80\ \mathrm{GeV/c^2}]$ and hard $[m_{\tilde{t}_1} = 150\ \mathrm{GeV/c^2}, m_{\tilde{\nu}} = 50\ \mathrm{GeV/c^2}]$ signal benchmarks as lines. Note that the WW events are concentrated in the first bin of the second plot. The $t\bar{t}$ events are concentrated in the third bin of the second plot. The $Z \to \tau\bar{\tau}$ events remaining after the selection cuts are in the first and second bins of the left plot. In the figures, the signal histograms are not stacked on top of the background histograms. The soft signal does not have any events with $S_T > 220$ GeV.

the efficiencies for the soft and hard signals are 6% and 17% respectively. After the two analysis cuts, the efficiencies fall to 3% and 15% respectively. However, these cuts achieve their intended result of reducing the $Z \to \tau\bar{\tau}$ and QCD backgrounds by 97% and 99% respectively. The electron and muon momentum distributions after the selection cuts are shown in Figures 6 and 7.

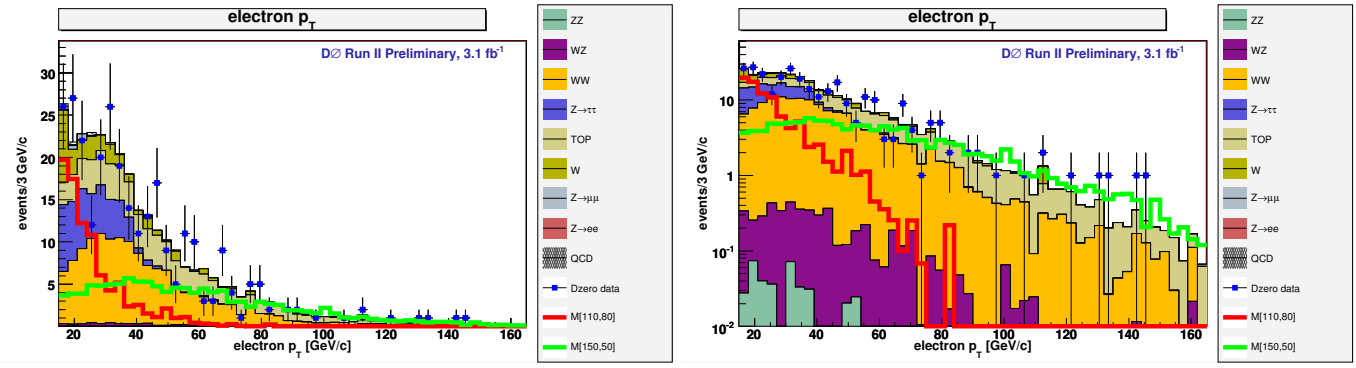

FIG. 6: Electron p_T distribution after the selection cuts in normal and log scale for data (points) and Monte Carlo plus QCD (filled areas). Also shown are the soft $[m_{\tilde{t}_1} = 110\ \mathrm{GeV/c^2}, m_{\tilde{\nu}} = 80\ \mathrm{GeV/c^2}]$ and hard $[m_{\tilde{t}_1} = 150\ \mathrm{GeV/c^2}, m_{\tilde{\nu}} = 50\ \mathrm{GeV/c^2}]$ signal benchmarks (lines).

VI. SYSTEMATIC UNCERTAINTIES

The signal cross section theoretical uncertainties, as discussed in Section III, are approximately 20% and are the dominant uncertainties in this analysis. The uncertainty on the integrated luminosity is 6.1%. A trigger efficiency uncertainty of 17% is applied to Monte Carlo events in which the electron has a p_T of less than 25 GeV/c, as determined from a data/Monte Carlo comparison for $Z \to \tau\tau$ events with low p_T electrons. For Monte Carlo events with p_T larger than 25 GeV/c, a trigger efficiency uncertainty of 6% is applied, as determined from $Z \to ee$ events. Since this analysis does not require events to have jets, the uncertainties of the jet energy scale and jet energy resolution primarily affect the distributions of events in the samples with minor effect on the number of events.

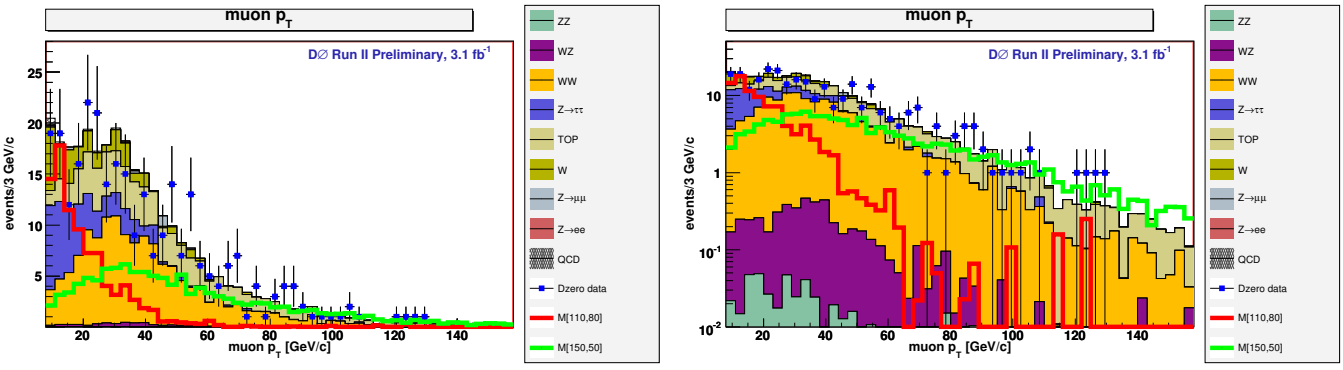

FIG. 7: Muon p_T distribution after the selection cuts in normal and log scale for data (points) and Monte Carlo plus QCD (filled areas). Also shown are the signal soft $[m_{\tilde{t}_1} = 110\ \mathrm{GeV/c^2}, m_{\tilde{\nu}} = 80\ \mathrm{GeV/c^2}]$ and hard $[m_{\tilde{t}_1} = 150\ \mathrm{GeV/c^2}, m_{\tilde{\nu}} = 50\ \mathrm{GeV/c^2}]$ signal benchmarks (lines).

	Cut 0: Preselection	**Cut 1: Angular differences**		**Cut 2: $\not\!\!E_T$**		
sample	**events**	**events**	eff.	**events**	eff.	combined eff.
ZZ	1 ± 11	0.6 ± 0.4	0.47	0.4 ± 0.2	0.71	0.32
WZ	$8\ ^{+1}_{-1}$	5 ± 1	0.72	$5\ ^{+0.5}_{-0.6}$	0.86	0.63
WW	$181\ ^{+17}_{-20}$	$161\ ^{+15}_{-18}$	0.89	$138\ ^{+13}_{-15}$	0.84	0.76
$Z \to \tau\bar{\tau}$	$1434\ ^{+104}_{-147}$	$536\ ^{+39}_{-56}$	0.37	$47\ ^{+4}_{-5}$	0.27	0.03
$t\bar{t}$	$121\ ^{+13}_{-17}$	$84\ ^{+9}_{-11}$	0.69	$80\ ^{+8}_{-11}$	0.94	0.66
W	$36\ ^{+4}_{-4}$	$33\ ^{+3.4}_{-4}$	0.91	$29\ ^{+3}_{-4}$	0.87	0.79
$Z \to \mu\bar{\mu}$	14 ± 12	5 ± 0.6	0.34	2 ± 0.3	0.53	0.15
$Z \to e\bar{e}$	12 ± 12	7 ± 1	0.6	0.3 ± 0.1	0.18	0.02
QCD	107 ± 63	53 ± 31	0.49	2 ± 1.0	0.11	0.01
BG total	$1905\ ^{+121}_{-161}$	$880\ ^{+52}_{-67}$	0.46	$303\ ^{+16}_{-20}$	0.37	0.16
data	1925	807	0.43	288	0.36	0.15
(150,50)	$161\ ^{+19}_{-21}$	$129\ ^{+15}_{-17}$	0.80	$122\ ^{+14}_{-16}$	0.93	0.76
(110,80)	$195\ ^{+24}_{-29}$	$140\ ^{+17}_{-21}$	0.72	$89\ ^{+11}_{-13}$	0.63	0.46

TABLE II: Summary of the selection cuts and their efficiencies. The efficiencies of each cut applied individually are shown. The last column gives the combined cut1 × cut2 efficiencies.

VII. RESULTS AND CONCLUSIONS

Limits were calculated using the TLimit software of the ROOT package[12] which is an implementation of the CLs Method[13]. TLimit incorporates the experimental uncertainties such as the uncertainty in the signal acceptance, the luminosity, and the trigger efficiency. The limits shown are for the central value of the theoretical prediction for the top squark cross section. No significant excess above the standard model prediction was found. We have set 95% confidence level exclusion limits for light top squark pair production assuming a 100% branching fraction to $b\bar{b}l^{\pm}l^{\mp}\tilde{\nu}\bar{\tilde{\nu}}$. We use these to set limits in the sneutrino mass versus stop mass plane as shown in Figure 8 and have excluded stop pair production for $m_{\tilde{t}_1} < 200$ GeV when $m_{\tilde{\nu}} < 110$ GeV and the difference $m_{\tilde{t}_1} - m_{\tilde{\nu}} > 30$ GeV. Also shown are earlier results from DØ using the combined ee+$e\mu$ channels and an independent 1.1 fb^{-1} sample [14], and the results from LEP [15], [16].

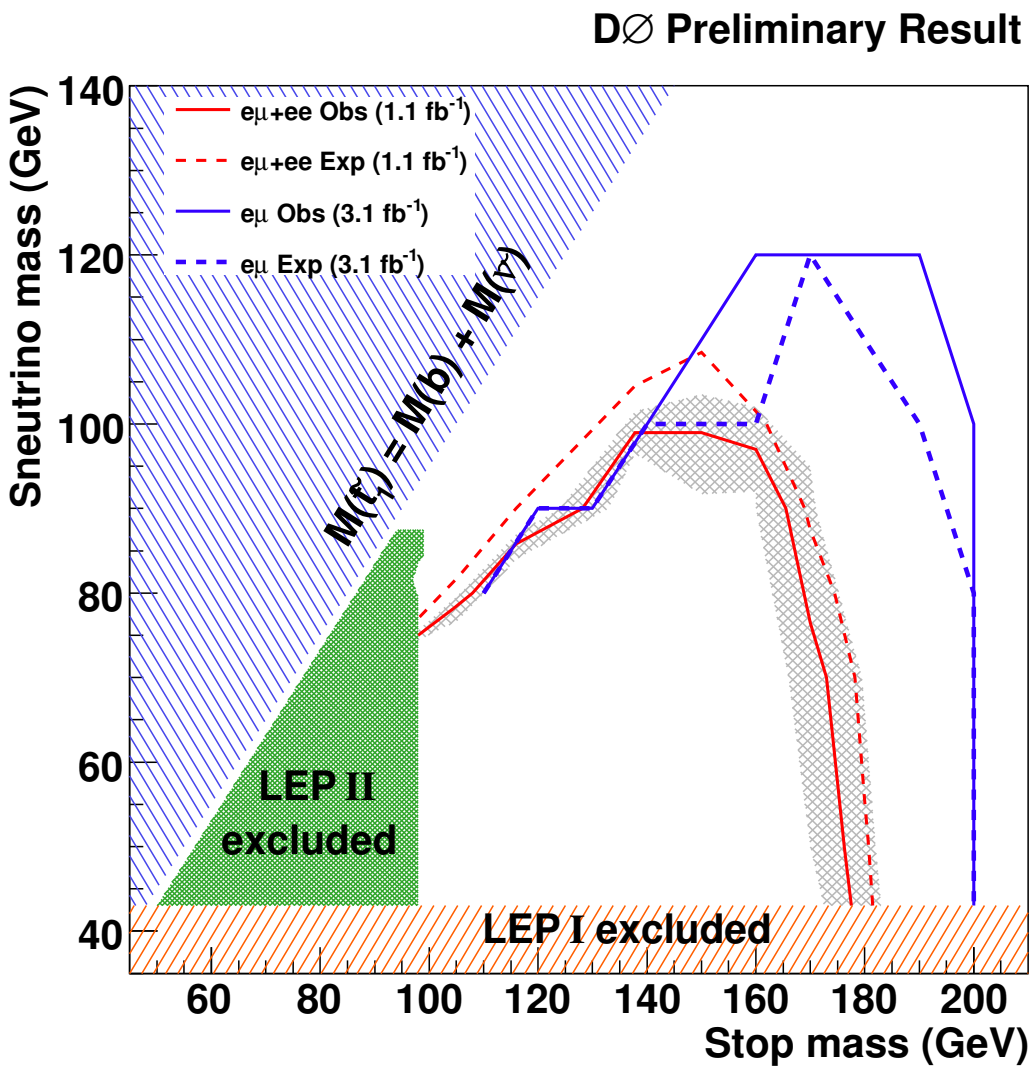

FIG. 8: The DØ 3.1 fb^{-1} preliminary observed (expected) 95% confidence level exclusion region includes all mass points below the solid (dashed) blue line. The shaded blue region is kinematically forbidden. The shaded orange and green areas were excluded by LEP I and LEP II respectively. Also shown is the DØ 1.1 fb^{-1} combined result from the $e\mu$ and ee channels. The grey band around the observed limit shows the effects of the top squark production cross section uncertainty.

Acknowledgments

We thank the staffs at Fermilab and collaborating institutions, and acknowledge support from the Department of Energy and National Science Foundation (USA), Commissariat à l'Energie Atomique and CNRS/Institut National de Physique Nucléaire et de Physique des Particules (France), Ministry of Education and Science, Agency for Atomic Energy and RF President Grants Program (Russia), CAPES, CNPq, FAPERJ, FAPESP and FUNDUNESP (Brazil), Departments of Atomic Energy and Science and Technology (India), Colciencias (Colombia), CONACyT (Mexico), KRF (Korea), CONICET and UBACyT (Argentina), The Foundation for Fundamental Research on Matter (The Netherlands), PPARC (United Kingdom), Ministry of Education (Czech Republic), Natural Sciences and Engineering Research Council and WestGrid Project (Canada), BMBF (Germany), A.P. Sloan Foundation, Civilian Research and Development Foundation, Research Corporation, Texas Advanced Research Program, and the Alexander von Humboldt Foundation.

---

[1] S. Dimopoulos and H. Georgi, Nucl. Phys. B **193**, 150 (1981).
[2] V. M. Abazov et al. (D0 Collaboration), Nucl. Instrum. Methods A **565**, 463 (2006).
[3] A. Djouadi, J.-L. Kneur, and G. Moultaka, Comput. Phys. Commun. **176**, 426 (2007).
[4] J. Alwall et al., JHEP **09**, 028 (2007).
[5] T. Sjostrand, S. Mrenna, and P. Skands, JHEP **05**, 026 (2006).
[6] W. Beenakker, R. Hopker, and M. Spira, hep-ph/9611232 (1996).
[7] J. Pumplin, D. R. Stump, J. Huston, H. L. Lai, P. Nadolsky, and W. K. Tung, JHEP **0207**, 12 (2002).
[8] D. Stump, J. Huston, J. Pumplin, W.-K. Tung, H. L. Lai, S. Kuhlmann, and J. F. Owens, JHEP **0310**, 046 (2003).
[9] M. L. Mangano, M. Moretti, F. Piccinini, R. Pittau, and A. D. Polosa, JHEP **07**, 001 (2003).
[10] S. Moch and P. Uwer, Nucl. Phys. Proc. Suppl. **183**, 75 (2008).
[11] G. C. Blazey et al., hep-ex/0005012 (2000).
[12] R. Brun, F. Rademakers, P. Canal, I. Antcheva, and D. Buskulic, *Tlimit in root package (see http://root.cern.ch/root/html/tlimit.html).*
[13] T. Junk, Nucl. Instrum. Methods A **434**, 435 (1999).
[14] V. M. Abazov et al. (D0 Collaboration), Phys. Lett. B **659**, 500 (2008).
[15] C. Amsler et al. (Particle Data Group), Phys. Lett. B **667**, 1 (2008).
[16] LEP SUSY Working Group (ALEPH, DELPHI, L3, and OPAL), **LEPSUSYWG/01-02.1** (2001), URL `http://lepsusy.web.cern.ch/lepsusy/`.